International Journal of Mechanical and Electrical Engineering
ISSN: 3005-9615 (Print), ISSN: 3005-7132 (Online) | Volume 7, Number 1, Year 2025
DOI: https://doi.org/10.62051/ijmee.v7n1.03
Journal homepage: https://wepub.org/index.php/IJMEE/index

Measurement and Analysis of Deformation Field Near the Tip of Mode-I Crack in Styrene-Butadiene Rubber

Huan Liu, Xiaohua Tan *

School of Mechanical Engineering, Tianjin University of Technology and Education, Tianjin, China
* Corresponding Author: Xiaohua Tan (Email: 1121093688@qq.com)

ABSTRACT

To study fracture mechanics in elastomeric materials, digital image correlation (DIC) was used to characterize the deformation field near the crack tip in industrial styrene-butadiene rubber. The sectoral distribution and strain singularity near the crack tip were systematically examined under different loading levels. Experimental results indicated that the crack-tip region was divided into an Expansion Sector (EX) and two Shrinking Sectors (SH). The EX angle increased with the applied load and eventually converged to approximately $\theta \approx \pm 32.5°$. Moreover, the strain field near the crack tip demonstrated singular behavior, characterized by three distinct layers: a nonlinear singular layer, an exponential singular layer, and a linear elastic layer. The singularity exponent of the exponential layer remained constant under increasing load, suggesting that the applied load amplified the strain magnitude without changing the intrinsic singularity behavior. These results validate the applicability of the fan-shaped sectoring theory for analyzing large-deformation fracture in styrene-butadiene rubber.

KEYWORDS

Large Deformation Fracture; Digital Image Correlation (DIC); Sectoring Configuration; Strain Field Singularity.

1. INTRODUCTION

In engineering applications, rubber materials frequently experience complex stress states that can initiate and propagate cracks, resulting in eventual failure. Understanding the distribution of the crack-tip deformation field and its interaction with crack propagation behavior is a key scientific challenge for enhancing the reliability of rubber components.

For metallic materials, linear elastic or elastoplastic fracture mechanics can precisely characterize the crack-tip field and predict fracture behavior. However, the hyperelasty, large deformation, and highly nonlinear mechanical response of rubber materials preclude the direct application of classical fracture theories [1]. The complexity of the constitutive behavior, in particular, substantially complicates both theoretical analysis and numerical simulation of the crack-tip field.

In the field of rubber fracture mechanics, researchers have performed systematic studies using theoretical, experimental, and numerical methods. Early work by Rivlin and Thomas [2] established a classical theoretical framework for fracture in elastomers using energy balance principles, providing the foundation for later studies. Recent advances in experimental techniques have enabled the widespread use of high-resolution methods—including optical microscopy, digital image correlation (DIC), and X-ray computed tomography—for measuring crack-tip fields in rubber [3–5]. Theoretically, Stephenson et al. [6] derived asymptotic solutions for Mode-I and Mode-II crack-tip

fields in rubber under plane strain conditions. Using a state-based peridynamic model, Zhou and Yao [7–8] systematically analyzed large deformation and fracture in compressible hyperelastic materials under quasi-static and dynamic loading. Numerically, the finite element method, incorporating constitutive models like Ogden and Yeoh, has been widely used to simulate crack propagation in rubber [9–10]. For example, Lin Xiaoshan et al. [11] successfully simulated the propagation of pre-existing cracks in short-fiber-reinforced rubber composites via the extended finite element method (XFEM). Xing C et al. [12] applied a phase-field modeling approach to simulate large deformation and failure in hyperelastic materials.

Most approaches depend primarily on a single mapping function and thus fail to accurately represent full-field deformation throughout the crack-tip region. The sectoring theory introduced by Gao Yuchen et al. [13] provides a promising alternative for addressing this limitation. This theory partitions the crack-tip field in rubber into expansion sector and shrinking sector, each described by a distinct mapping function, enabling more accurate representation of stress/strain distributions under large deformations. However, experimental validation and in-depth analysis of this sectoring structure remain scarce, and its coupling with crack propagation behavior has not been fully elucidated. In this paper, Digital Image Correlation (DIC) was applied to measure deformation fields near the crack tip in rubber. The sectoring features and their evolution are systematically examined to establish a more accurate predictive framework for rubber fracture mechanics.

2. MEASUREMENT OF CRACK TIP DEFORMATION FIELD IN STYRENE-BUTADIENE RUBBER

2.1. Sample Preparation and Loading

Commercial styrene-butadiene rubber sheets with a thickness of 2 mm were used as the test material. Specimens were cut to dimensions of 58 mm × 34 mm and clamped at both ends with metal fixtures, as shown in Fig. 1. To prevent slippage or gripping-induced fracture, elastic rubber gaskets were placed between the fixture and specimen surfaces. The gaskets both protected the specimen and improved clamping stability.

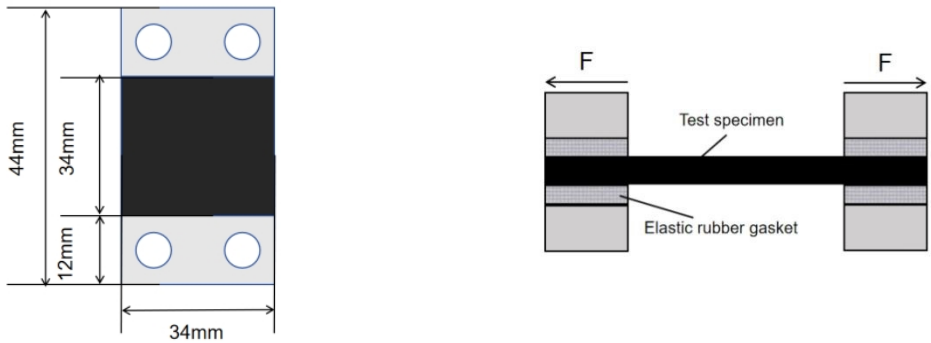

(a) (b)

Fig 1. Schematic diagram of the tensile specimen: (a) front view; (b) side view.

An IBTC-300SL micro in-situ mechanical testing system (Kaili Measurement and Control Technology, Tianjin) was used for tensile testing. The system has a load capacity of 0.01–300 N and a displacement range of 150 mm. The experimental setup is shown in Fig. 2.

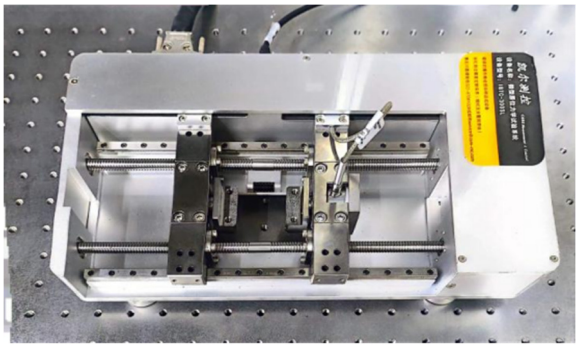

Fig 2. Schematic of the micro in-situ mechanical testing system.

2.2. DIC Experimental Protocol

Preliminary tensile tests were conducted to determine the typical deformation range of the styrene-butadiene rubber under operational conditions. Based on the measured deformation, the camera's field of view (FOV) was set to 60 mm × 60 mm.

A CCD camera with a resolution of 1000 × 1000 pixels, a focal length of 25 mm, and a pixel size of 2.5 μm was employed. The corresponding sensor size was calculated as $2.5\mu m \times 1000 = 2.5mm$. The working distance was determined from the FOV using the following formula:

$$\frac{Focal\ length}{Object\ distance} = \frac{Target\ surface}{Field\ of\ view} \tag{1}$$

Let the distance between objects be A, then

$$A = \frac{Focal\ length \times Field\ of\ view}{Target\ surface} \tag{2}$$

Substitute the data to obtain

$$A = \frac{25mm \times 60mm}{2.5mm} = 600mm$$

The speckle diameter was determined from the field of view and the camera resolution. To ensure accurate DIC measurements, each speckle must cover 3–5 pixels. Excessively large speckles reduce discriminable features in each subset, increasing random errors. Conversely, speckles that are too small can cause image undersampling and introduce significant interpolation-induced errors. Due to the large-deformation characteristics of rubber, a speckle size covering 5 pixels was selected. Denoting this length as B, the speckle diameter is calculated as follows:

$$B = \frac{Field\ of\ view\ length}{1000} \times 5 = \frac{60}{1000} \times 5 = 0.3mm \tag{3}$$

Conventional spray-painting techniques typically yield speckles with inconsistent sizes, which are susceptible to detachment under large deformations. To address these issues, digitally designed speckle patterns were produced and transferred onto the specimen surface to precisely control speckle size and enhance adhesion.

The Mode-I fracture behavior of the styrene-butadiene rubber was investigated using a digital image correlation (DIC) system integrated with an IBTC-300SL micro in-situ mechanical testing system. The experimental configuration is presented in Fig. 3. The observation area measured 34 mm × 34 mm and contained a centered, prefabricated single-edge crack measuring 8 mm in length, as depicted in Fig. 4.

The camera position was aligned based on the calculated working distance. The CCD camera featured a resolution of 1000 × 1000 pixels and an exposure time of 100 μs. The tensile test was conducted at a constant crosshead speed of 2 mm/min (0.033 mm/s), and the loading direction was normal to the crack line. Images were acquired synchronously at a rate of 2 frames per second (fps).

After testing, the captured images were imported into DIC software for analysis. A region of interest around the crack tip was selected with a step size of 1 and a subset size of 13. A low-pass filter was applied to reduce noise before extracting displacement and strain fields.

Fig 3. Photograph of the experimental setup

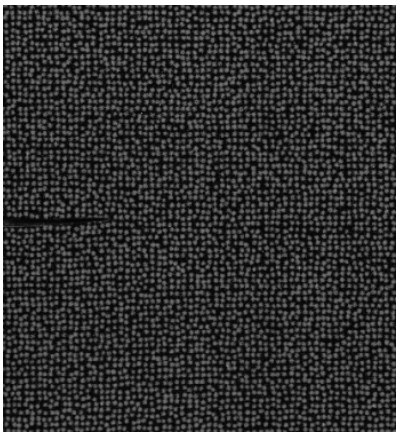

Fig 4. Speckle pattern on a styrene-butadiene rubber specimens with a prefabricated crack

3. FRACTURE TIP DISPLACEMENT FIELD PARTITIONING CONFIGURATION AND STRAIN SINGULARITY ANALYSIS

3.1. Displacement Field Analysis

The displacement field in the Cartesian coordinate system was derived from DIC software analysis. It was then transformed into radial displacement u_r and circumferential displacement u_θ by applying coordinate transformation formula (4).

$$\begin{cases} u_r = u\cos\theta + v\sin\theta \\ u_\theta = v\cos\theta - u\sin\theta \end{cases} \tag{4}$$

As an example, Fig. 8 illustrates the displacement field contour under 26 N. A clear zero-isoline of radial displacement u_r was identified near $\theta \approx \pm 22.5°$, suggesting negligible radial displacement of material points in this region. Inside the region bounded by the zero-isoline, u_r remained negative, indicating movement of material points toward the crack tip. Outside this region, where $u_r > 0$, material points displaced away from the crack tip.

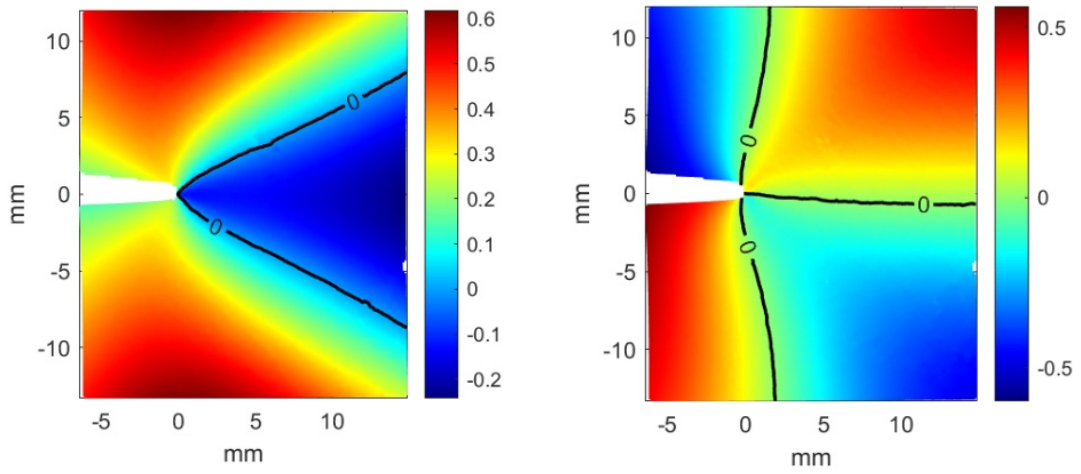

Fig 5. Contour plots of the radial displacement field u_r and the circumferential displacement field u_θ

A clearly visible zero-isoline was identified in the circumferential displacement field u_θ, occurring near $\theta \approx 0°$ and $\theta \approx \pm 80°$, which implies negligible displacement of material points in the circumferential direction within these zones. For $\theta > 0°$, positive values of u_θ were observed, corresponding to counterclockwise rotation around the crack tip. For $\theta < 0°$, negative values suggested clockwise rotation and an overall tendency for outward expansion. Furthermore, near $\theta \approx \pm 80°$, the material exhibited inward contraction.

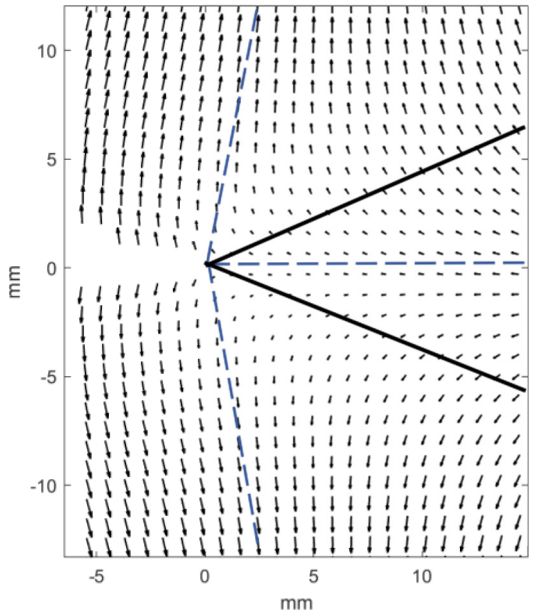

Fig 6. Resultant displacement vector field in the polar coordinate system.

To better characterize material point motion near the crack tip, the resultant displacement field was derived from the radial and circumferential displacement components. The resultant vector field (Fig. 6) clearly demonstrates that within the sector $\theta \approx \pm 22.5°$, material points displace toward the crack tip, predominantly due to circumferential expansion. This region is defined as the Expansion Sector (EX). In contrast, outside this sector ($\theta > 22.5°$ or $\theta < -22.5°$), material points exhibit circumferential contraction while moving away from the crack, defining the Shrinking Sector (SH).

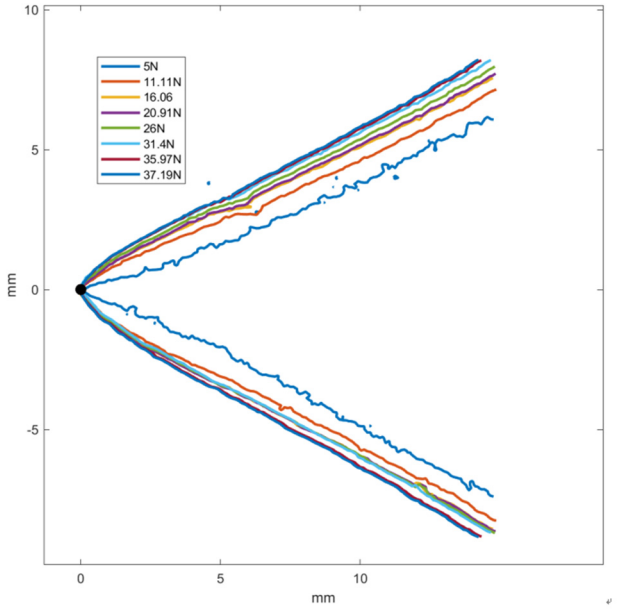

Fig 7. Zero-isoline characteristics under different load levels.

To observe the evolution of the sectoring angle in styrene-butadiene rubber prior to crack propagation, the crack initiation point was monitored using a CCD camera. The corresponding maximum load was identified as 37.19 N. The zero-isolines of displacement were then extracted and compared at load intervals of approximately 5-6 N.

As shown in the figure, the sectoring angle increased rapidly with the applied load in the initial stage, followed by a more gradual rise in later stages, eventually stabilizing around $\theta \approx \pm 32.5°$. This indicates that the sectoring angle expands with increasing load until it reaches a maximum boundary near $\theta \approx \pm 32.5°$.

3.2. Analysis of Strain Field Singularities

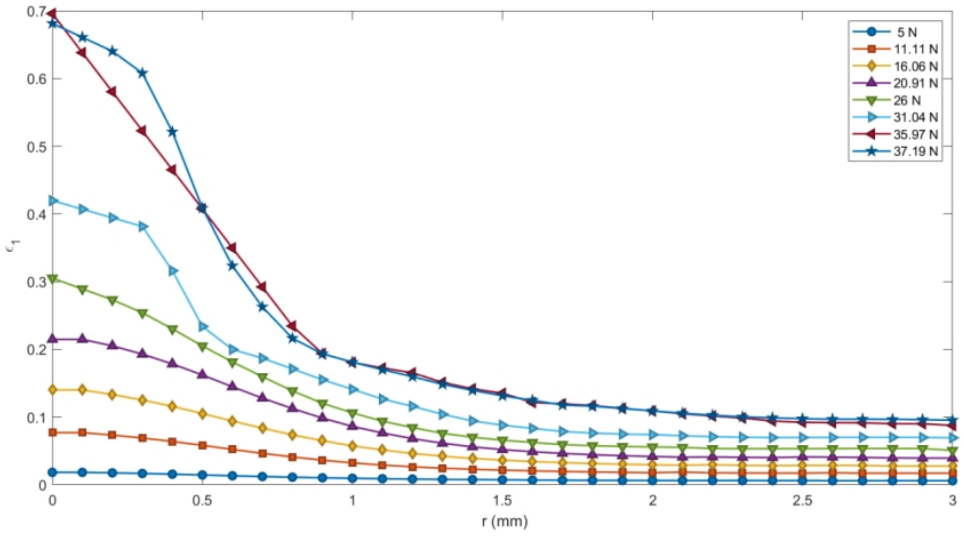

Fig 8. Strain (ε₁) vs. distance (r) at different load levels

As shown in Fig. 8, all curves indicate a sharp increase in strain ε_1 as the distance r from the crack tip decreases, consistent with the singular nature of the crack-tip strain field. Near $r = 0$, the strain rises rapidly, indicating a high strain gradient in the immediate vicinity of the crack tip. In the far-field region ($r > 2$ mm), the strain stabilizes and remains relatively constant.

With increasing load, the overall strain level rises, and the strain values in the near-tip region increase significantly, suggesting intensified plastic deformation under higher loads. The abnormal strain observed at 37.19 N indicates the onset of localized damage.

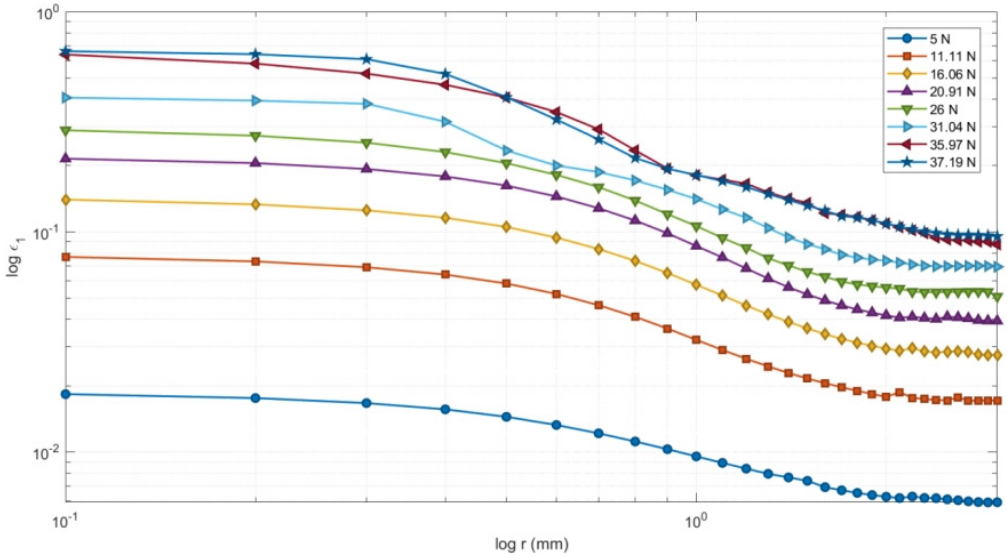

Fig 9. log(ε₁) vs. log(r) at different load levels.

To quantify the singularity characteristics, the strain distribution is presented in a double-logarithmic coordinate system in Fig. 9. The results reveal that the singular zone near the crack tip can be divided into three distinct layers: an innermost nonlinear singular layer, an intermediate layer exhibiting exponential-type singularity, and an outer linear elastic layer. As the load increases, the singularity exponent, represented by the slope of the intermediate layer, remains virtually unchanged. This indicates that while higher loads amplify the strain response of the material, they do not alter the nature of the strain singularity.

4. SUMMARY

This study investigated the sectoring configuration of the displacement field and the strain singularity at the Mode I crack tip in styrene-butadiene rubber using digital image correlation (DIC). The main conclusions are summarized as follows:

The experimental results confirm that the crack-tip region can be divided into an Expansion Sector (EX) and two Shrinking Sectors (SH), characterized by material points moving toward or away from the crack tip, respectively. As the load increased from 5 N to 37.78 N, the sectoring boundary angle expanded significantly from an initial $\theta \approx \pm 22.5°$ to a stabilized value of approximately $\theta \approx \pm 32.5°$. This indicates that higher loads enlarge the deformation zone without altering the fundamental sectoring configuration. These findings provide robust experimental support for Gao Yuchen's sectoring theory under large deformation conditions in rubber, offering a visual characterization of crack propagation behavior.

The strain distribution near the crack tip exhibits a three-layer singular structure: an inner nonlinear singular layer, an intermediate layer with exponential variation, and an outer linear elastic layer. The singularity exponent of the intermediate layer remains constant under increasing load. This indicates that the load amplifies the strain magnitude without altering the intrinsic nature of the singularity.

CONFLICTS OF INTEREST

The authors declare that they have no conflict of interest.

ACKNOWLEDGMENTS

This research was financially supported by the National Natural Science Foundation of China (11702193).

REFERENCES

[1] Zhang Y G. Influence of cross-sectional geometry on the Poynting effect in hyperelastic circular tubes[D]. Xi'an University of Technology, 2024..

[2] Rivlin R S, Thomas A G. Rupture of rubber. I. Characteristic energy for tearing[J]. Journal of polymer science, 1953, 10(3): 291-318.

[3] Lin W J, Gao Q, Chen D D, et al. Dynamically bonded self-healing polymer electrolytes: molecular design and characterization[J/OL]. Chinese Science Bulletin, 1-17[2025-08-30].

[4] Garcea S C, Mavrogordato M N, Scott A E, et al. Fatigue micromechanism characterisation in carbon fibre reinforced polymers using synchrotron radiation computed tomography[J]. Composites science and technology, 2014, 99: 23-30.

[5] Sun P. Influence of hydrogen bonding on the crack resistance of epoxidized natural rubber[D]. Hubei University, 2024..

[6] Stephenson R A,The equilibrium field near the tip of a crack for finite plane strain of incompressible elastic materials,Journal of Elasticity,1982,12:65-99.

[7] Zhou X P, Yao W W. Smoothed bond-based peridynamics[J]. Journal of Peridynamics and Nonlocal Modeling, 2022, 4: 452-474.

[8] Yao W , Zhou X P. Numerical modelling of compressible hyperelasticity via smoothed state-based peridynamics[J]. Engineering Analysis with Boundary Elements, 2022, 140: 476–493.

[9] Chen P, Li Z, Wu Z, et al. Temperature and crack path deviation effects on fatigue crack growth of a noncrystallizing rubber[J]. Rubber Chemistry and Technology, 2025, 98(1): 142-154.

[10] Zhang X Y, Jia J H, Gao S S, et al. Mechanical properties and crack propagation damage in finite element simulation of carbon fiber/rubber and carbon black/rubber composites[J]. Polymer Materials Science and Engineering, 2024, 40(07): 94-102.

[11] Lin X S, Yang X X, Gao J H. Crack propagation analysis of short fiber/rubber composites based on the extended finite element method[J]. Chinese Journal of Solid Mechanics, 2022, 43(01): 81-94.

[12] Xing C, Yu T, Sun Y, Wang Y. An adaptive phase-field model with variable-node elements for fracture of hyperelastic materials at large deformations[J]. Engineering Fracture Mechanics, 2023, 281: 109115.

[13] Gao Y C, Jin M, Dui G S, et al. Stress state description, singularity problems and complementary energy principle in elastic large deformation[J]. Advances in Mechanics, 2011, 41(01): 93-113.